ELSEVIER

Journal of Alloys and Compounds 281 (1998) 249–263

Journal of ALLOYS AND COMPOUNDS

Liquid–solid equilibria in the Al-rich corner of the Al–Mn–Cr system

T. Schenk[1,a], M. Durand-Charre[a], M. Audier[b,*]

[a]*Laboratoire de Thermodynamique et Physico-Chimie Métallurgiques (U.M.R. CNRS 5614), E.N.S.E.E.G., BP75, 38402 Saint Martin d'Hères, France*
[b]*Laboratoire des Matériaux et du Génie Physique, UMR CNRS 5628, ENSPG. BP46, 38402 Saint Martin d'Heres, France*

Received 13 July 1998

Abstract

The aspect of the Al–Mn–Cr phase diagram related to liquid–solid equilibria in the subsection Al_4Cr–Al_4Mn–Al was investigated. It is shown that ternary $Al_4Mn_xCr_{1-x}$ compounds ($0 \leq x \leq 1$) whose structure correspond to that of the hexagonal μAl_4Mn phase, previously identified as a periodic approximant of Al–Mn and Al–Cr quasicrystalline phases, are in equilibrium with a liquidus phase field extending between both binary Al–Mn and Al–Cr limits. A new ternary Al–Mn–Cr phase, called Ψ, is also found and characterised. Its structure is monoclinic with cell parameters $a_\Psi = 17.48$ Å, $b_\Psi = 30.31$ Å, $c_\Psi = 24.695$ Å, $\beta = 135°$ and a space group of either *C2/c* or *Cc* symmetry . But as peculiar structural faults are observed in this monoclinic Ψ-phase, its formation is assumed to be the result of an allotropic transformation of an orthorhombic structure which would first solidify. Besides, from structural relationships observed between the μ and Ψ structures, it is suggested that the atomic structure of Ψ could also be typical of an arrangement of icosahedral clusters as, for instance, those defined in both the μAl_4Mn and $\lambda Al_{4.5}Mn$ structures.

Keywords: Al–Mn–Cr alloys; Ternary phase diagram; Quasicrystalline; Icosahedral clusters

1. Introduction

Several crystallographers such as Samsom [1,2], Brink-Shoemaker and Shoemaker [3,4] have pointed out that a common feature of several complex Al-transition metal structures is the occurrence of similar local icosahedral units formed by one transition metal surrounded by 12 atoms, mainly Al atoms situated at the vertices of slightly distorted icosahedra. Transition metals (TM) are in that case either Mn, Cr, Fe, Co, V, W, Re, Tc or Mo. Such a local order has also been proposed in related amorphous and liquid phases and is presumed to be present in the structure of Al–Mn and Al–Cr quasicrystalline phases discovered by Shechtman, Blech, Gratias and Cahn [5]. Recently, the general characteristic of this local icosahedral order was confirmed in different studies of the atomic structure of intermetallic compounds of very large cell parameters: $\lambda Al_{4.5}Mn$ [6], κAlNiCr [7] and $Al_{5.1}(Fe,Cr)$ [8].

The fact that icosahedral units seem to be particularly stable irrespective of whether there is a long range order or not, has been interpreted as resulting from the strong stability of the icosahedral units [9] where the calculated relative stability of isolated $Al_{12}TM$ clusters as a function of the 3d series TM was found to be maximum for Mn and Cr, i.e. precisely TM atoms for which binary Al–TM quasicrystals seem only to be obtained. Therefore, the role played by such a cluster in the physical properties of solid and liquid phases should be interesting to elucidate. For instance, a correlation effect between local icosahedral order and paramagnetic properties of liquid Al–Mn and Al–Pd–Mn alloys has recently been suggested [10] for which a few attempts of interpretation are proposed in theoretical works [11–14].

In the present metallurgical study of the Al-rich corner of the Al–Mn–Cr system, we were interested to determine whether liquid Al–Mn–Cr alloys could be used for further investigations of the local icosahedral order in liquid phases. The first reason being that if an isomorphic substitution between Mn and Cr occurs in liquid Al–Mn–Cr alloys, then it should be possible to obtain from neutron scattering experiments, the partial distribution functions $g_{Al-Al}(r)$, $g_{Al-TM}(r)$ and $g_{TM-TM}(r)$ for a complete description of the liquid structure because the neutron scattering lengths by Cr and Mn atoms are very different (i.e. 0.3635 and −0.373 fm, respectively) and important contrast

*Corresponding author.

[1] Present address: Institut für Raumsimulation, DLR, D-51170 Köln, Ruhr-Universität Bochum, D-44780 Bochum, Germany.

0925-8388/98/$ – see front matter
PII: S0925-8388(98)00787-7

effects can be expected for an accurate determination of these functions. Although it can only be assumed, but not proved, that an isomorphic substitution might occur in liquid phases (e.g. this has been assumed between Mn atoms and a Fe–Cr atomic mixture in liquid Al–Pd–Mn–Fe–Cr and Al–Mn–Fe–Cr alloys [15–17]), there are particular cases where such a behaviour is very likely. When an isomorphic substitution occurs in solids, then it provides a convincing argument for inferring that it occurs as well in liquids in equilibrium with these solids. A priori, such a property could be expected in Al–Mn–Cr alloys because both binary Al–Mn [18,19] and Al–Cr [20,21] systems exhibit solidification reactions giving rise to the formation of isomorphic hexagonal structures μAl_4Mn [22,23] and μAl_4Cr [21,24,25]. Moreover, the possibility of a liquid-$\mu Al_4Cr_xMn_{1-x}$ phase equilibrium with a Mn/Cr isomorphic substitution in the μ-structure can also be considered as ideal for further neutron scattering studies of the equilibrium liquid Al–Mn–Cr alloys because the μ-structure exhibits a local icosahedral order [21,23] and the chemical composition of both μAl_4Mn and μAl_4Cr compounds correspond to those of icosahedral phases but are only obtained by rapid quenching.

The results reported in this article deal with the determination of Al–Cr–Mn liquidus–solidus equilibria, in particular, that of a liquid-μ phase equilibrium with a continuous variation of the Mn/Cr ratio. A brief recall is made about previous reported results on neutron powder diffraction and magnetisation studies [26] indicating that the Mn/Cr substitution in $\mu Al_4Cr_xMn_{1-x}$ compounds ($0 \leq x \leq 1$) is isomorphic. The structural characterisation of a new ternary Al–Cr–Mn phase is presented and of its relations with binary Al–Mn and Al–Cr intermetallic structures are discussed.

1.1. Experimental procedure

The study of the phase diagram related to liquid–solid equilibria in the subsection Al_4Cr–Al_4Mn–Al was carried out in two steps:

(i) The formation of the μ-phase was verified from the study of a first set of five alloys (Table 1a) from which the position of a peritectic line limiting the liquidus phase field of this phase on the Mn and Cr-rich side was approximately determined.

(ii) Liquid–solid equilibria were then specified from the study of a second set of seven alloys (Table 1b). These latter, whose compositions were chosen very close to the peritectic boundary determined in the first step, were then used for fabrications by Bridgman growth of different $\mu Al_4Mn_xCr_{1-x}$ phase compounds with $0 \leq x \leq 1$.

All these alloys were prepared by melting high purity constituent elements (99.99%) in an inductive cold crucible under argon atmosphere. The seven alloys indicated in Table 1b were re-melted in alumina crucibles and under argon atmosphere for Bridgman growths.

The crystallisation sequences were deduced from SEM and TEM observations and liquidus temperatures of six alloys were measured by differential thermal analysis (DTA) of samples of about 1 g. The cooling and heating rates were 5°C min^{-1} or less. A few experiments were stopped by quenching at the appearance of the first solid phase in order to determine the first compound to be formed. Isothermal sections of the phase diagram were determined from analyses of samples annealed at various temperatures for 40 min and rapidly quenched in water. The composition of the phases were first determined approximately by X-ray energy dispersive spectroscopy in a scanning electron microscope (SEM) and then accurately by X-ray wavelength spectroscopy on a Cameca SX50 microprobe (EPMA). The atomic compositions were established using the ZAF modified PAP correction program [27]. Different phase structures were identified by electron diffraction and high resolution imaging using a transmission electron microscope (TEM). Specimens were prepared as thinned foils by ion milling or as fine powders by crushing small pieces of alloy ingots, which were deposited onto copper grids coated with a carbon film. The μ-phase structure of compounds containing different Mn/Cr ratios was also verified by X-ray powder diffraction. All

Table 1
(a) and (b): Sets of initial compositions of the alloys with crystallisation sequences as deduced from SEM and TEM observations and temperatures of liquidus (T_L) observed by DTA

	Alloy	Phases in the order of appearance	T_L (°C)	Ref.
(a)	$Al_{81}Cr_{0.76}Mn_{18.2}$	$Al_{11}Mn_4$, μ, Al_6Mn, Al_6Mn/(Al)	–	
	$Al_{85}Cr_{3.75}Mn_{11.25}$	type $Al_{11}Mn_4$, μ, Al_6Mn, Al_6Mn/(Al)	–	
	$Al_{85}Cr_{7.5}Mn_{7.5}$	type $Al_{11}Mn_4$, μ, η, Ψ, Ψ(Al), Al_6Mn/(Al)	–	
	$Al_{85}Cr_{11.25}Mn_{3.75}$	type Al_9Cr_4, μ, η, θ, (Al)	–	
	$Al_{83.8}Cr_{15.41}Mn_{0.78}$	Al_9Cr_4, μ, η, θ, (Al)	–	
(b)	$Al_{88}Mn_{12}$	μ, Al_6Mn, Al_6Mn/(Al)	896	[9]
	$Al_{88.65}Cr_{1.75}Mn_{9.6}$	$Al_{11}Mn_4$, μAl_6Mn/(Al)	910	[7]
	$Al_{88.2}Cr_{3.8}Mn_8$	μ, Ψ, Ψ(Al), Al_6Mn/(Al)	980	[6]
	$Al_{88}Cr_6Mn_6$	μ, η, Ψ, Ψ(Al), Al_6Mn/(Al)	1005	[1,2]
	$Al_{87.25}Cr_{9.75}Mn_3$	type Al_9Cr_4, μ, η, η/(Al), Ψ(Al), Al_6Mn/(Al)	1015	[5]
	$Al_{87.1}Cr_{10.7}Mn_{2.2}$	μ, η, θ, (Al)	–	[8]
	$Al_{87.5}Cr_{12.5}$	Al_9Cr_4, μ, η, θ, (Al)	1022	[3,4]

The reference numbers indicated in the last column are related to those indicated in Fig. 1 (d). The notation for the eutectic phase is given as Al_6Mn/(Al).

these μ-phase Bridgman samples have also been used for a study on the nature of the Mn/Cr substitution by neutron powder diffraction and magnetic susceptibility measurements using a SQUID (Superconducting Quantum Interference Device) [26].

2. Phase equilibria

Several intermetallic phases mainly formed by peritectic reactions were considered from the data on both binary phase diagrams Al–Mn [18,19] and Al–Cr [20,21]. Their structures are recalled in Table 2 containing also a ternary Ψ-phase presently identified. As preliminary investigations from a first set of five alloys (Table 1a), SEM observations of the as-cast microstructure of the alloys $Al_{85}Cr_{11.25}Mn_{3.75}$ $Al_{85}Cr_{7.5}Mn_{7.5}$ and $Al_{85}Cr_{3.75}Mn_{11.25}$, revealed a primary crystallisation of large faceted grains of Widmanstatten-like precipitates embedded in an Al matrix. The structure of these precipitates were found by TEM to correspond to this of the orthorhombic ηAl_5Cr phase within each alloy. Their compositions as measured by XEDS were found to be related to a Mn/Cr substitution in the ηAl_5Cr phase and in which the Mn/Cr ratios were quite close to those of the initial alloys. Other phases ($Al_{11}Mn_4$, Al_9Cr_4, μ, Ψ, θ) were also observed in these as-cast microstructures but in small proportions. Formation of μ-compounds containing different Mn/Cr ratios were only obtained as majority phase after annealing treatments, at 1000°C for the $Al_{81}Cr_{0.76}Mn_{18.2}$ and $Al_{85}Cr_{11.25}Mn_{3.75}$ alloys and at 900°C for the $Al_{85}Cr_{7.5}Mn_{7.5}$, $Al_{85}Cr_{3.75}Mn_{11.25}$ and $Al_{83.8}Cr_{15.41}Mn_{0.78}$ alloys. From DTA analyses and TEM observations, primary crystallisations of compounds of either $Al_{11}Mn_4$ structure in the Mn-rich alloys or Al_9Cr_4 structure in the Cr-rich alloys were observed as preceding the formation of μ-compounds (Table 1a). Then, the position of a peritectic line limiting the liquidus phase field of this phase on the Mn and Cr-rich side was roughly estimated from this first study. Note that with respect to previous observations [21] on Al–Cr alloys having 17, 20 and 25 at.% Cr, the nucleation behaviours of both the η and μ phases appear to be different because the formation of ηAl_5Cr phase has not been detected in as-cast Al–Cr samples but only through slow cooling (3°C min^{-1}). For these as-cast Al–Cr alloys, the crystallisation sequences were always Al_9Cr_4, μAl_4Cr followed by θAl_7Cr, while for the as-cast Al–Cr–Mn alloys presently studied, η-compounds nucleate much more easily as metastable phase than stable Al_9Cr_4 or $Al_{11}Mn_4$ phases and the μ-phase is only formed in large proportion through further annealing treatments.

Since the existence of a continuous μ-phase region bounded by μAl_4Mn and μAl_4Cr could be expected from these first results, we have prepared a second set of alloys (Table 1b) in order to fabricate by Bridgman growth several pure μ-phase compounds containing different Mn/Cr ratios. In their as cast state, a metastable crystallisation of the η-phase was again found in all ternary alloys but not in both binary $Al_{88}Mn_{12}$ and $Al_{87.5}Cr_{12.5}$ alloys. On account of the microstructure observed by SEM on samples either analysed by DTA or annealed at temperatures of 700, 750 or 800°C for 40 min and rapidly quenched in water, the crystallisation paths were determined (Table 1b). For three alloys ($Al_{87.5}Cr_{12.5}$, $Al_{87.25}Cr_{9.75}Mn_3$ and $Al_{88.65}Cr_{1.75}Mn_{9.6}$) the proportion of transition metal was slightly too important for yielding a primary crystallisation of μ-phase; its formation was preceded by this of Al_9Cr_4 or $Al_{11}Mn_4$. The crystallisation of a ternary Ψ-phase from the liquid was observed in three alloys ($Al_{87.25}Cr_{9.75}Mn_3$, $Al_{88.65}Cr_6Mn_6$ and $Al_{88.2}Cr_{3.8}Mn_8$) and also through

Table 2
Crystallographic data on the phases considered in the present study

Phase	Bravais lattice	Space group	Cell parameters (Å)	Ref.
Al	Cubic	$Fm\bar{3}m$	$a=4.049$	
$Al_{12}Mn$	Cubic	$Im\bar{3}$	$a=7.47$	[28]
Al_6Mn	Orthorhombic	*Cmcm*	$a=7.5518$, $b=6.4978$, $c=8.8703$	[29]
$\lambda Al_{4.5}Mn$	Hexagonal	$P6_3/m$	$a=28.382$, $c=12.389$	[6]
μAl_4Mn	Hexagonal	$P6_3/mmc$	$a=19.98$, $c=24.673$	[22]
πAl_4Mn (metastable)	Orthorhombic (type $Al_{60}Mn_{11}Ni_4$)	*Bbmm*	$a=23.6$, $b=12.4$, $c=7.7$ Å	[30]
$\phi Al_{10}Mn_3$	Hexagonal	$P6_3/mmc$	$a=7.54$, $c=7.90$ Å	[31]
$Al_{11}Mn_4$ (or Al_3Mn)	Orthorhombic	*Pnma*	$a=14.8$, $b=12.42$, $c=12.59$	[32]
$Al_{11}Mn4$ (high T form)	Triclinic	$P\bar{1}$	$a=5.095$, $b=8.879$, $c=5.05$ $\alpha=89.35°$, $\beta=100.47°$, $\gamma=105.08°$	[33]
$\theta Al_{45}Cr_7$	Monoclinic (type $Al_{45}V_7$)	$C2/m$	$a=25.256$, $b=7.582$, $c=10.955$ $\beta=128.68°$	[34]
ηAl_5Cr or $Al_{11}Cr_2$	Orthorhombic	*Cmcm* or $Cmc2_1$ or *Ama2*	$a=12.35$, $b=34.6$, $c=20$	[21]
μAl_4Cr	Hexagonal (type μAl_4Mn)	$P6_3/mmc$	$a=20.076$, $c=24.80$	[26]
Al_9Cr_4	Cubic		$a=9.123$	[35]
$\Psi Al_{82}Cr_{2.3}Mn_{15.7}$	Monoclinic	$C2/c$ or *Cc*	$a=17.48$, $b=24.72$, $c=30.31$ $\beta=135°$	p.w.

annealing treatments, at 700°C for the $Al_{88.65}Cr_{1.75}Mn_{9.6}$ alloy and at 750°C for the $Al_{88.2}Cr_{3.8}Mn_8$ and $Al_{88.65}Cr_{1.75}Mn_{9.6}$ alloys. From the results on chemical composition and structure analyses isothermal sections at 700, 750 and 800°C were plotted (Fig. 1a,b,c and Table 3). As shown in these sections there are different ternary equilibria occurring between a liquid phase and two intermetallic compounds, namely liquid $\Psi+Al_6Mn$, liquid

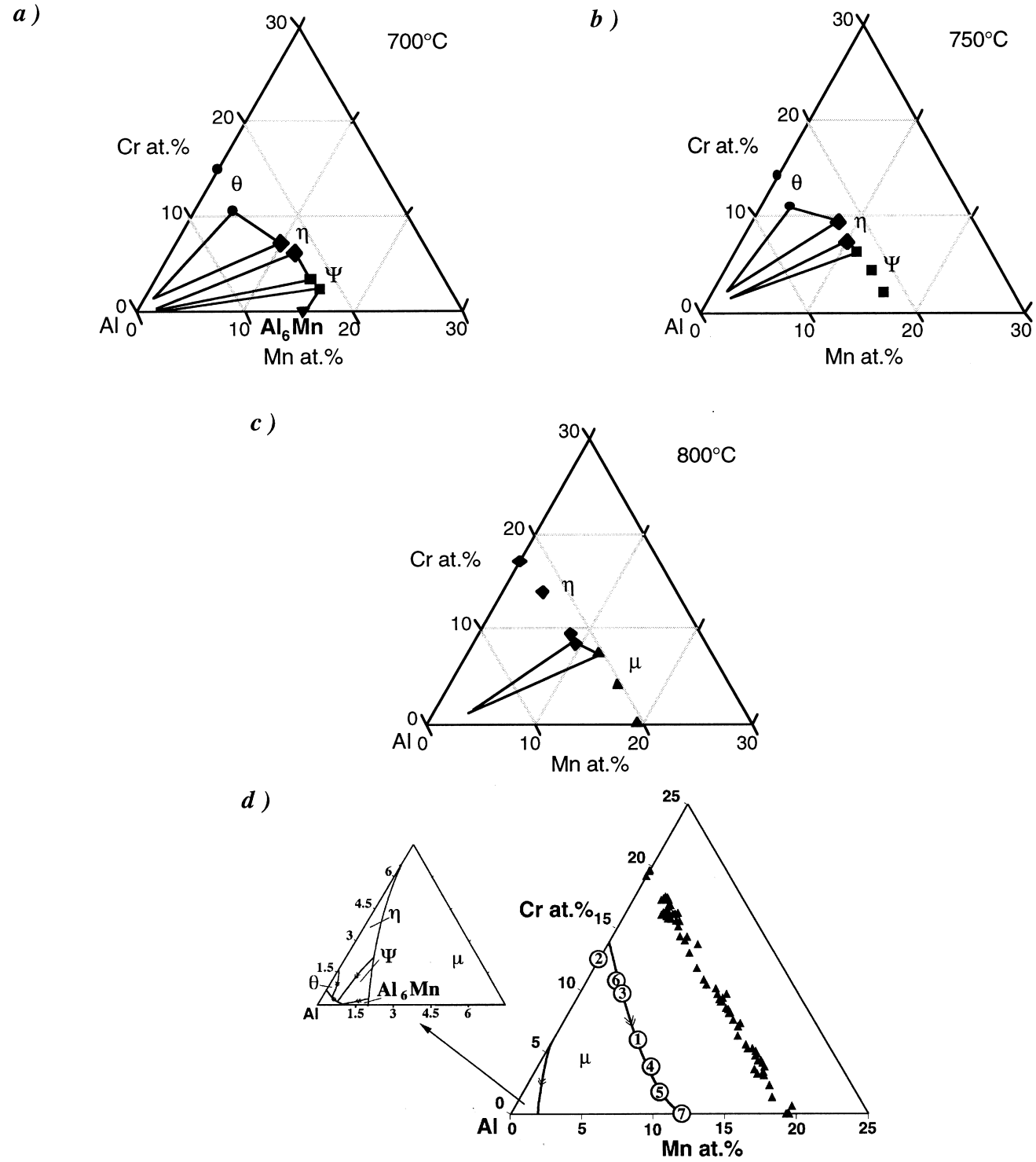

Fig. 1. Isothermal sections of the Al–Cr–Mn system at 700°C (a), 750°C (b) and 800°C (c) where different ternary equilibria occur between a liquid phase and two intermetallic compounds: liquid $\Leftrightarrow\Psi+Al_6Mn$, liquid $\Leftrightarrow\Psi+\eta$ and liquid $\Leftrightarrow\eta+\theta$ at 700°C; liquid $\Leftrightarrow\Psi+\eta$ and liquid $\Leftrightarrow\eta+\theta$ at 750°C; liquid $\Leftrightarrow\mu+\eta$ at 800°C; (d) projection of liquidus phase fields where the μ-phase compositions and initial alloy compositions (open circles with reference numbers corresponding to those indicated in Table 1) are reported.

Table 3
Average chemical composition of phases corresponding to different equilibria occurring at 700, 750 and 800°C. The composition of liquids have been estimated from SEM analyses, by measuring the proportions of the equilibrium solid phases

	Al at.%	Mn at.%	Cr at.%
Isothermal section at 700°C			
Ψ-Al_6Mn – Liquid equilibrium			
Al_6Mn	84.6	15.4	0
Ψ	82	15.7	2.3
liquid	98	1.95	0.05
Ψ–η – Liquid equilibrium			
Ψ	82.4	14.2	3.4
η	82.3	11.5	6.2
liquid	97.9	1.7	0.4
η–θ – Liquid equilibrium			
η	83	9.9	7.1
θ	85.7	3.6	10.7
liquid	97.8	1	1.2
θ – Liquid equilibrium			
θ	85	0	15
Isothermal section at 750°C			
Ψ – Liquid equilibria			
Ψ	82.1	15.8	2.1
Ψ	82	13.6	4.4
Ψ–η – Liquid equilibrium			
Ψ	82.3	11.3	6.4
η	82.7	9.8	7.5
Liquid	96.5	2.1	1.4
η–θ – Liquid equilibrium			
η	82.5	7.9	9.6
θ	86.1	2.8	11.1
Liquid	96.5	1.3	2.2
θ – Liquid equilibrium			
θ	85.8	0	14.2
Isothermal section at 800°C			
μ – Liquid equilibria			
μ	80.7	19.3	0
μ	80.5	15.5	4
μ–η – Liquid equilibrium			
μ	80.5	12	7.5
η	82	9.5	8.5
Liquid	95	3.6	1.4
η – Liquid equilibria			
η	82	8.5	9.5
η	82.4	3.7	13.9
η	82.8	0	17.2

$\Leftrightarrow\Psi+\eta$ and liquid $\Leftrightarrow\eta+\theta$ at 700°C; liquid $\Leftrightarrow\Psi+\eta$ and liquid $\Leftrightarrow\eta+\theta$ at 750°C; liquid $\Leftrightarrow\mu+\eta$ at 800°C. For instance, the SEM micrograph of Fig. 2 is related to the coexistence of both the Ψ- and η-phases which were in equilibrium with a liquid phase at 700°C in the $Al_{88.7}Cr_{1.8}Mn_{9.6}$ alloy sample. Therefore, taking account of all these crystallisation paths and isothermal equilibria, determined from the solidification of different alloys and the measured liquidus temperatures, we propose in Fig. 1d, a scheme for the projection of liquidus phase fields limited to the subsection Al_4Mn–Al_4Cr–Al. The compositions of the initial alloys and those of the μ-compounds are given in this diagram; the small liquidus phase fields corresponding to a primary crystallization of the θ, η, Ψ and Al_6Mn phases respectively are indicated in an enlarged part of this diagram where it can be noticed that the solidification ends at the binary eutectic Al_6Mn/Al. Note that the line separating the liquidus phase field of Al from the liquidus phase fields of the θ, η, Ψ and Al_6Mn phases is peritectic on the Al–Cr side and becomes an eutectic valley towards the Al–Mn side. Intermediate transformations of pseudo-peritectic nature occur along this line: Al+liquid+θ→Al+liquid+η; Al+liquid+η→Al+liquid+Ψ and Al+liquid+Ψ→Al+liquid+Al_6Mn.

All the alloys indicated in Table 1b were successively re-melted in alumina crucibles in a Bridgman furnace. For each sample (of about 60 g), a formation of μ-phase was obtained on 50 to 60% of the length of the Bridgman ingot. Very small quantities of other compounds were however observed at the grain boundaries of the μ-phase (grain sizes of several millimetres). Due to an evolution of composition of non-congruent liquid–solid equilibria as a function of temperature, each ternary μ-sample exhibited a variation in their Mn and Cr concentrations along the Bridgman ingot length. The range of variation of the ratio $x=C_{Mn}/(C_{Mn}+C_{Cr})$ and for each sample are reported in Table 4. Note that in accordance with the results of the analyses of DTA samples, primary crystallisations of either $Al_{11}Mn_4$ from the liquid $Al_{88.65}Cr_{1.75}Mn_{9.6}$ alloy or Al_9Cr_4 from the liquid $Al_{87.25}Cr_{9.75}Mn_3$ and $Al_{87.5}Cr_{12.5}$ alloys were first formed as a very thin layer (30 to 50 μm) in the corresponding Bridgman ingots. Thus, such results confirmed that the position of a upper peritectic limit for the μ-phase formation was quite correctly determined in the first step of our study.

3. Structures

3.1. μ-Compounds

The different μ-phase compounds obtained by Bridgman growth were reduced into powders for X-ray and neutron diffraction experiments. From X-ray powder diffraction, performed using the Cu Kα radiation, we have found that each sample spectrum exhibited the reflection positions corresponding to those of the hexagonal μAl_4Mn structure. Slight variations in the reflection intensities and in the hexagonal cell parameters have also been observed as a function of the different Mn/Cr ratios of samples. However, as atomic scattering factors of Cr and Mn are very close (for instance, f_{Mn}/f_{Cr} varies only from 1.0416 to 1.0646 between 0 and 1.5 $Å^{-1}$), the relative reflection intensity variations observed as a function of the different Mn/Cr ratios in μ-phase samples were too small for carrying out an accurate study on the nature of the Mn/Cr substitution, i.e. whether isomorphic or not.

This has been studied by neutron powder diffraction [26] because there is an important contrast between Mn

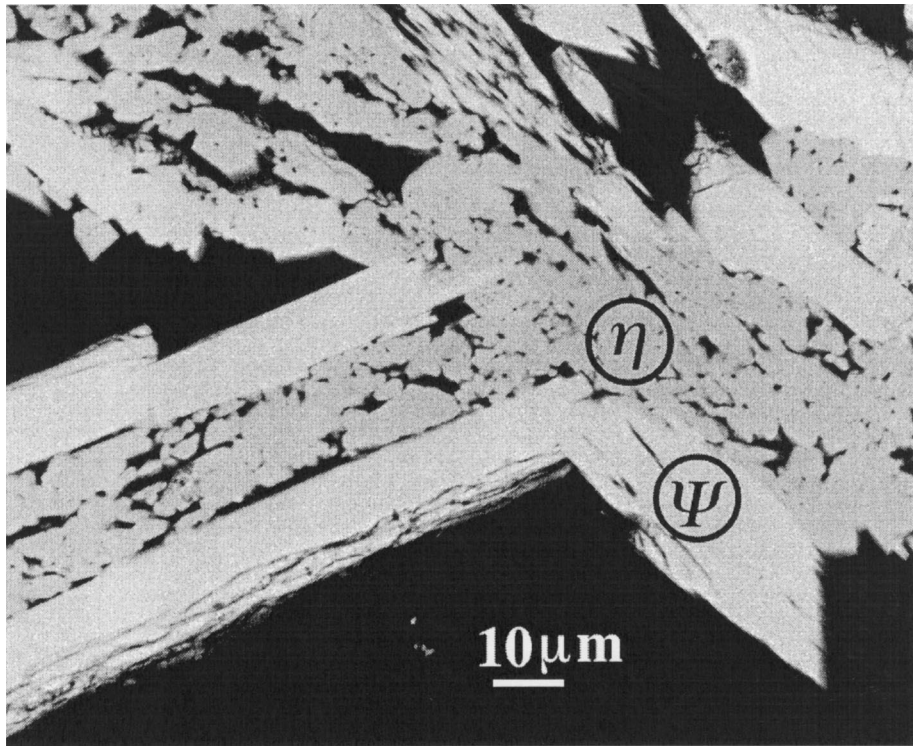

Fig. 2. SEM micrograph of a polished section of the $Al_{88.7}Cr_{1.8}Mn_{9.6}$ alloy sample annealed at 700°C and quenched. Both the Ψ and η-phases are observed to be embedded in an Al-rich matrix; the grain sizes and their arrangement is typical of a ternary equilibrium between both these phases and a liquid phase occurring at 700°C.

and Cr in that case; the neutron scattering lengths by Cr and Mn are respectively equal to 0.3635 and −0.373 fm, as previously mentioned. Let us recall that neutron diffraction spectra on all the μ-phase samples obtained by Bridgman growth have been measured at Laboratoire Léon Brillouin on the spectrometer G4.2 with a wavelength $\lambda=2.597$ Å selected with a graphite monochromator. About 750 reflections have been measured in a 2θ range of $5.522°\leq 2\theta \leq 151.837°$ (i.e. corresponding to a momentum transfer range $0.3606\ Å^{-1}\leq Q\leq 4.7075\ Å^{-1}$). The obtained spectra have been analysed using the FULLPROF program [36] which is based on the Rietveld method [37,38]. For instance, part of spectra obtained on both μAl_4Mn and μAl_4Cr compounds (i.e. for $20°\leq 2\theta \leq 120°$ corresponding to a total number of 590 reflections) are shown in Fig. 3 where for each sample the measured intensities, corrected of the background, are superimposed to calculated intensities from the structural model of Brink-Shoemaker et al. [22] which yields a good fit of the experimental data. Between both these spectra, many reflection intensities appear to be very different.

However, if the structural model of Brink-Shoemaker et al. [22] (i.e. the atomic coordinates, Debye-Waller and occupancy factors) has directly been applied in order to

Table 4
Range of variation of the ratio $x=C_{Mn}/(C_{Mn}+C_{Cr})$ determined for each μ-phase sample obtained by Bridgman growth

Alloy	Al at.%	x ratio variation through the μ-phase Bridgman ingot length						x_a
		0%	20%	40%	60%	80%	100%	
$Al_{88}Mn_{12}$	80.5	1	1	1	1	1	1	1
$Al_{88.65}Cr_{1.75}Mn_{9.6}$	81.0	0.93	0.88	0.84	0.81	0.78	0.76	0.83
$Al_{88.2}Cr_{3.8}Mn_8$	80.7	0.52	0.56	0.61	0.67	0.71	0.73	0.63
$Al_{88}Cr_6Mn_6$	80.9	0.32	0.38	0.43	0.48	0.53	0.58	0.45
$Al_{87.25}Cr_{9.75}Mn_3$	81.3	0.14	0.18	0.20	0.22	0.25	0.27	0.21
$Al_{87.1}Cr_{10.7}Mn_{2.2}$	81.2	0.11	0.14	0.15	0.16	0.17	0.18	0.16
$Al_{87.5}Cr_{12.5}$	80.8	0	0	0	0	0	0	0

Different per cent values of the Bridgman ingot lengths, where μ-phase compounds were observed, are given from the beginning to the end of crystallisation of this phase. As indicated in column 2, the Al concentration in each sample correspond to an average value of measured concentrations varying at about ±0.5 at.%. Average x_a values given in the last column are not exact but just indicative for a comparison with x ratios obtained from a refinement of neutron powder diffraction data (see Table 4).

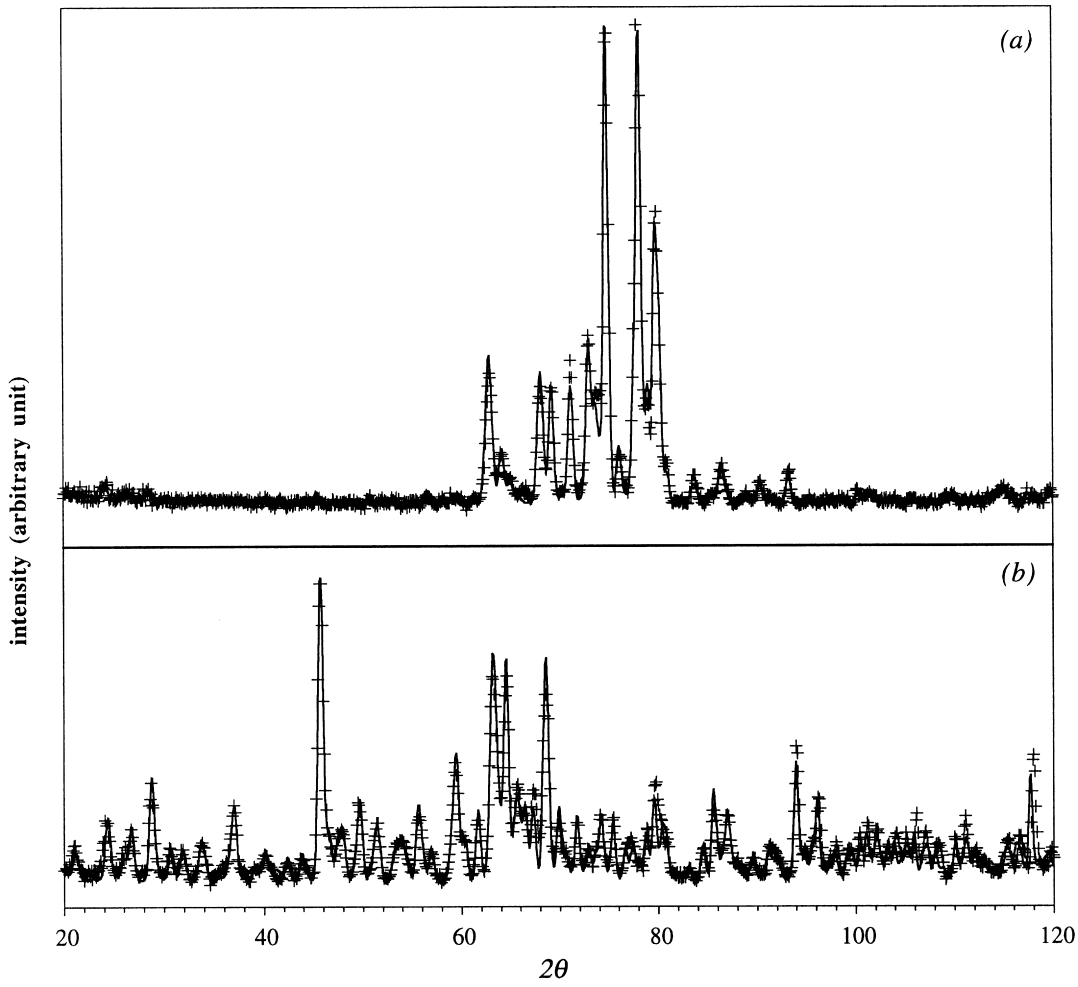

Fig. 3. Part of the neutron powder spectra observed (+) and calculated from the model of Brink-Shoemaker et al. [21] (———) for the Al_4Cr (a) and Al_4Mn (b) phases.

obtain such an agreement for the binary μAl_4Mn and μAl_4Cr compounds, the same procedure could not successfully be applied to the spectra of ternary compounds. A direct refinement of the Mn and Cr occupancy factors on all TM Wyckoff sites in the μ structure for identifying the nature of the Mn/Cr substitution, did not converge. The convergence to a solution was too sensitive to very small variations of these factors. Besides, there was an additional difficulty resulting from the Cr and Mn concentration variations in each sample (cf. Table 4). A good agreement between the measured and calculated intensities, has only been obtained by varying the relative proportions of Cr and Mn atoms within each μ compound but with the assumption that the Mn/Cr substitution ratios for all TM Wyckoff sites were identical (i.e. that the substitution is isomorphic). Through such a procedure, the refinement of the cell parameters showed a variation about linear as a function of the refined average ratios $x=C_{Mn}/(C_{Cr}+C_{Mn})$ in the μ phase samples (Table 5); a variation which is also in agreement with the condition that Cr atoms randomly replace Mn atoms slightly smaller than Cr atoms. Note that an isomorphic substitution behaviour between Mn and Cr has also been deduced to be in agreement with a linear variation of the magnetic susceptibility as a function of $C_{Mn}/(C_{Cr}+C_{Mn})$ measured on a SQUID [26]. Therefore, from neutron powder diffraction and magnetisation measurements it could well be concluded that an isomorphic Mn/Cr substitution is realised in this hexagonal $Al_4Mn_xCr_{1-x}$ phase in the range $0 \leq x \leq 1$.

Table 5
Neutron powder diffraction data on the crystallographic parameters as a function of the $C_{Mn}/(C_{Mn}+C_{Cr})$ ratios in μ-phase samples (from Ref. [20])

Alloy	$C_{Mn}/(C_{Mn}+C_{Cr})$	a (Å)	c (Å)
$Al_{88}Mn_{12}$	1	19.980	24.67
$Al_{88.65}Cr_{1.75}Mn_{9.6}$	0.823	20.000	24.69
$Al_{88.2}Cr_{3.8}Mn_8$	0.612	20.020	24.72
$Al_{88}Cr_6Mn_6$	0.407	20.035	24.74
$Al_{87.25}Cr_{9.75}Mn_3$	0.177	20.060	24.77
$Al_{87.1}Cr_{10.7}Mn_{2.2}$	0.164	20.060	24.78
$Al_{87.5}Cr_{12.5}$	0	20.076	24.80

3.2. Structure of the Ψ phase and relationships with binary phases

The structure of the Ψ-phase was found to be monoclinic (Table 2). Its Bravais lattice as deduced from electron diffraction patterns (Fig. 4a) is quite particular because it can be confused with a C orthorhombic lattice from the observed geometry of the diffraction patterns. The symmetries observed between intense reflections have to be considered in order to distinguish between the Laue class of an orthorhombic system (*mmm*) and that of a monoclinic system (*1 2/m 1*). For instance, considering the patterns of [010], [1$\bar{1}$0] and [$\bar{1}$00] zone axes related between them through a rotation about the *001* row (Fig. 4a), intense reflections are related by an horizontal mirror line on the pattern [$\bar{1}$00] but not on the patterns [010] and [1$\bar{1}$0]. Along the pattern of the [1$\bar{1}$0] zone axis, the intense reflections are only related by a centre of symmetry and along the [010] zone axis, they seem to be related by mirror planes σ1 and σ2 situated at 45° from the horizontal. Therefore, as the symmetries of the Laue class *mmm* are not respected, the case of an orthorhombic Bravais lattice must be excluded. A monoclinic Bravais lattice was then determined from the indexing of the diffraction patterns shown in Fig. 4a in a manner that the reflection conditions are in agreement with those of the space groups *Cc* (non-centrosymmetric) and *C2/c* (centrosymmetric), i.e. $h+k=2n$ for *hkl* and $l=2n$ for *001*. Note that *001* reflections with $l\neq 2n$ are observed in the diffraction pattern of the [1$\bar{1}$0] zone axis but they result from double diffraction effects as it can easily be verified from other diffraction patterns related by a rotation around this *001* row. The geometrical identity between the diffraction patterns of [001] and [$\bar{2}$01] zone axes results from a particular value of 135° for the β angle. Looking at a high resolution image of the Ψ-structure oriented along its [010] zone axis (i.e. parallel to the electron beam), the fringe pattern observed appears to be in agreement with the projection of the symmetry element of the *C2/c* space group (Fig. 4b). Nevertheless, although it confirms the possibility for such a centrosymmetric space group, the other possibility of a non-centrosymmetric space group *Cc* cannot be excluded.

Note that the symmetries related to mirror planes σ1 and σ2 between the diffraction patterns of [010], [001] and [$\bar{2}$01] zone axes are obviously not imposed by the symmetry elements of both these space groups. Meanwhile such additional symmetry elements means that a pseudo-merohedral twinning related to a mirror operation σ1, or equivalently σ2, might be envisaged. Twinned crystals were effectively observed (Fig. 5). In the top part of Fig. 5, the twinning occurs between two crystals belonging to a same sandwich layer perpendicular to the b_Ψ axis while in the bottom part, crystals belonging to different layers are related, not by twinning but by an equivalent operation for the resulting orientations, either the [100] or [101] zone axis. From such an observation, it can be assumed that the monoclinic structure of the Ψ-phase probably results from a phase transition of a C orthorhombic structure of which the space group could be either *Cmcm*, $Cmc2_1$ or *C*2*cm* if the reflection intensities are only changed in order to respect a Laue class of symmetry *mmm*. From such an assumption of the orthorhombic structure, which would only be stable at high temperature, both the observed orientations of the monoclinic structure have an equal probability to be formed on cooling.

The cell parameters of the monoclinic Ψ-structure were quite accurately determined because of an orientation relationship observed between both the μ and Ψ phases and from which the cell parameters of the μ-structure can be used as a reference scale. Fig. 6 shows a high resolution image of an interface observed between the μ and Ψ phases formed in the $Al_{88.65}Cr_{1.75}Mn_{9.6}$ alloy annealed at 700°C. The corresponding electron diffraction patterns are successively related, from the left to the right, to the μ-phase oriented along its [0001] zone axis, to the μ–Ψ interface and to the Ψ-phase oriented along its [201] or [001] zone axis (i.e. zone axes of orientation which cannot be distinguished neither by electron diffraction nor by high resolution imaging). The orientation relationship is:

$$[0001]_\mu // [001]_\Psi \text{ or } [201]_\Psi$$

$$\boldsymbol{a}_\mu \text{ or } [2\bar{1}\bar{1}1]_\mu // [201]_\Psi \text{ or } [001]_\Psi$$

$$[01\bar{1}0]_\mu // [010]_\Psi$$

From direct comparisons between distances measured on high resolution images related to this interface, we have deduced the following relations between the cell parameters of both structures:

$$(1.618)a_\Psi = a_\mu/\sqrt{2}$$

$$b_\Psi = (7a_\mu\sqrt{3})/8$$

$$c_\Psi = c_\mu$$

The last relation was verified on an image where the Ψ and μ phases from both sides of the interface exhibited a [201] and a [2$\bar{1}\bar{1}$0] zone axis, respectively.

Knowing the cell parameters of the μ-phase compound obtained from the $Al_{88.65}Cr_{1.75}Mn_{9.6}$ alloy ($a_\mu = 19.998$ Å, $c_\mu = 24.695$ Å), the cell parameters of this Ψ-phase compound, whose average composition is $Al_{82}Cr_{2.3}Mn_{15.7}$ from XWDS analyses on bulk samples of this alloy, were then deduced to be:

$$a_\Psi = 17.48 \text{ Å},\ b_\Psi = 30.31 \text{ Å},\ c_\Psi = 4.695 \text{ Å},\ \beta = 135°$$

As the Mn/Cr ratio is variable in the Ψ-phase, its cell parameters are probably depending on this ratio.

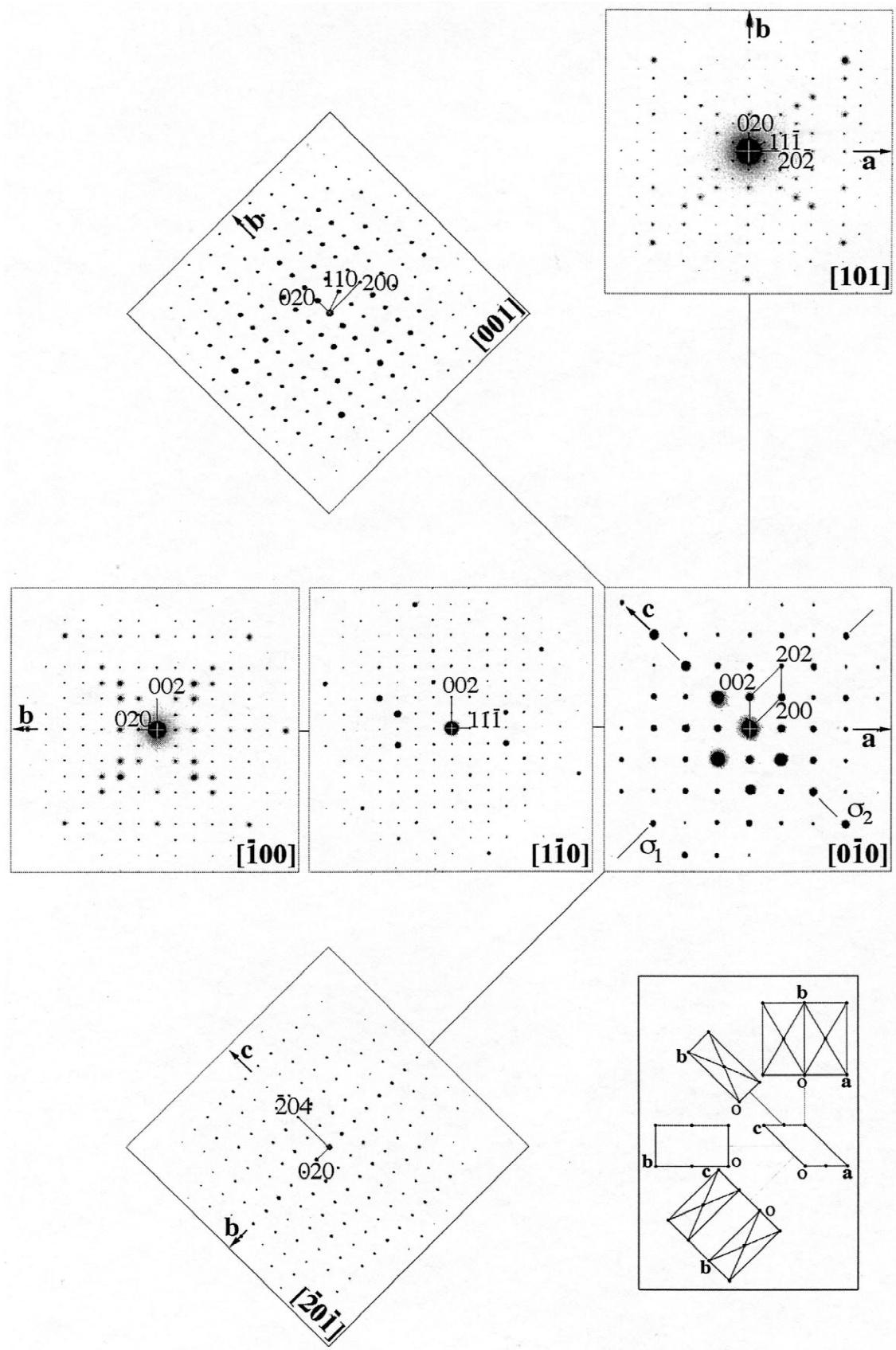

Fig. 4. Ψ-Structure: (a) Main electron diffraction patterns of the monoclinic Ψ-structure, the [101], [001], $[\bar{1}00]$ and $[\bar{2}0\bar{1}]$ are successively related between them by 45° rotations about the ***b*** axis and related to the $[0\bar{1}0]$ pattern by 90° rotations about *h01, h00, 001* and $\bar{h}021$ rows, respectively. A schema of the corresponding orientations of the monoclinic cell in the direct space is indicated in the right bottom part of this figure. As explained in Section 3.2, the Laue class of symmetry of such patterns is typical of a monoclinic system but not of an orthorhombic one. For instance, the $[1\bar{1}0]$ pattern situated in between those of $[0\bar{1}0]$ and $[\bar{1}00]$ zone axes is shown in order to point out that intense reflections are only related by a centre of symmetry; (b) lattice fringe image corresponding to the diffraction pattern of [010] zone axis from which it can be verified that its symmetry elements in agreement with those of the *C2/c* space group.

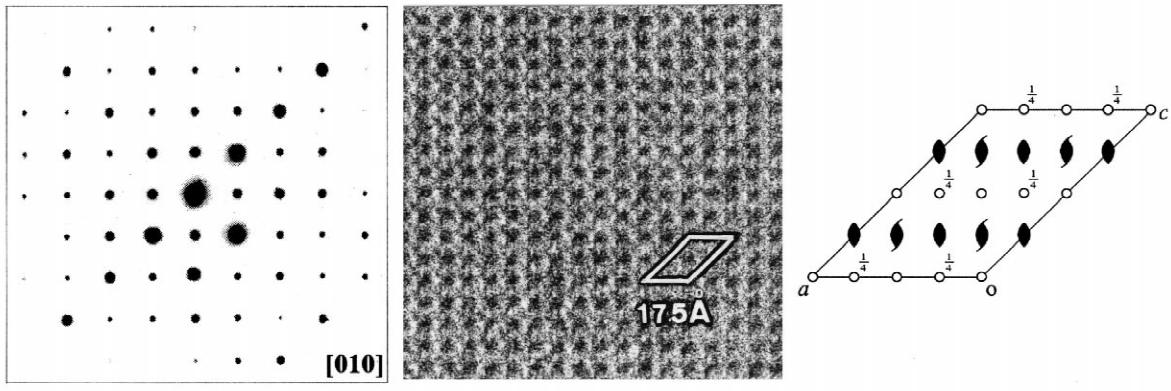

Fig. 4. (*continued*)

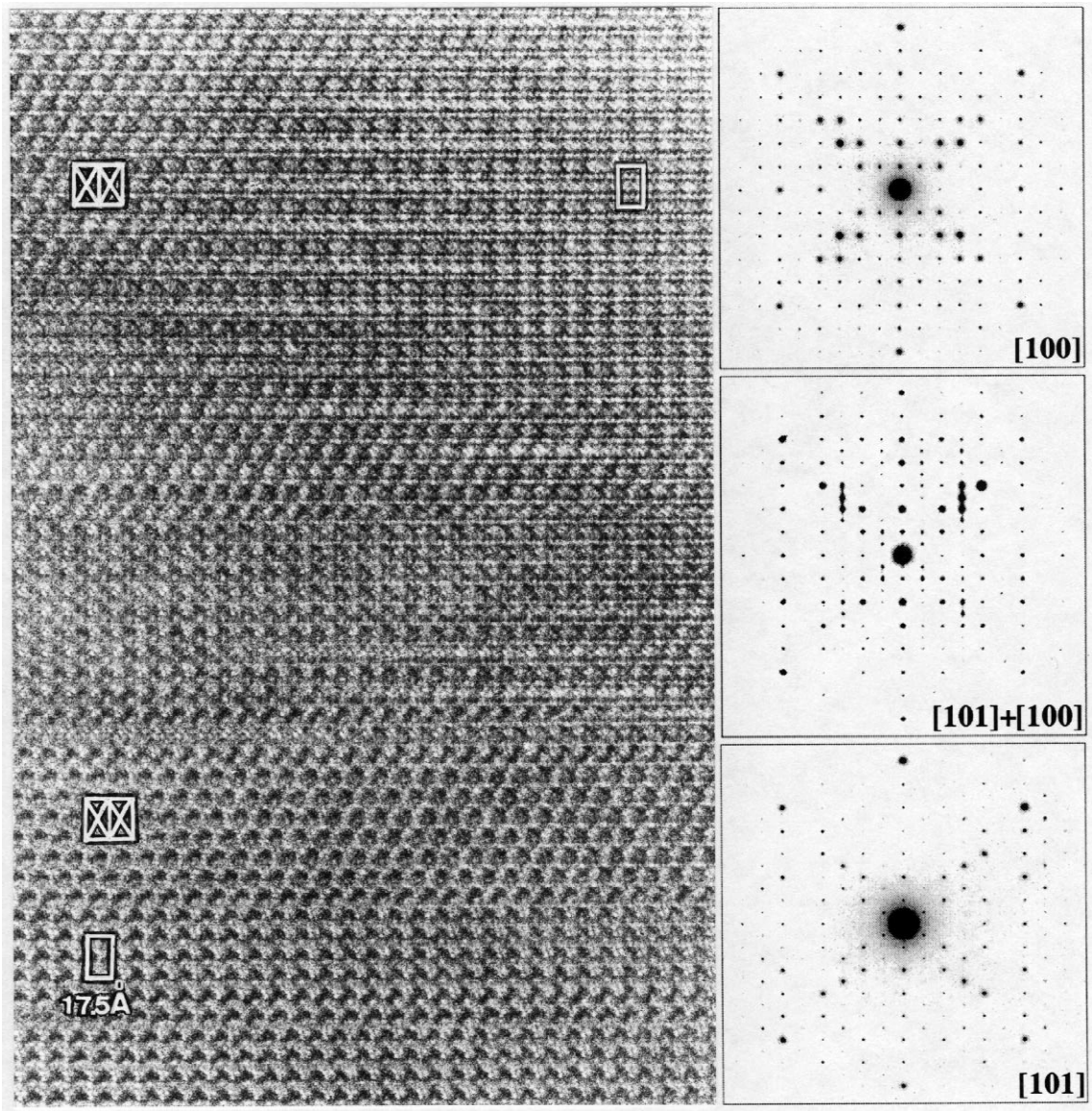

Fig. 5. Sandwich structure of the Ψ-phase corresponding to both orientations of observation [100] and [101]: A twinning occurs between two crystals belonging to a same sandwich layer perpendicular to the b_{Ψ} axis on the top part of the image while in the bottom part, crystals belonging to different layers are related, not by twinning but by an equivalent operation for the resulting orientations. The diffraction pattern corresponding to both orientations [100] and [101] shows that the distances between the reflection rows are exactly the same.

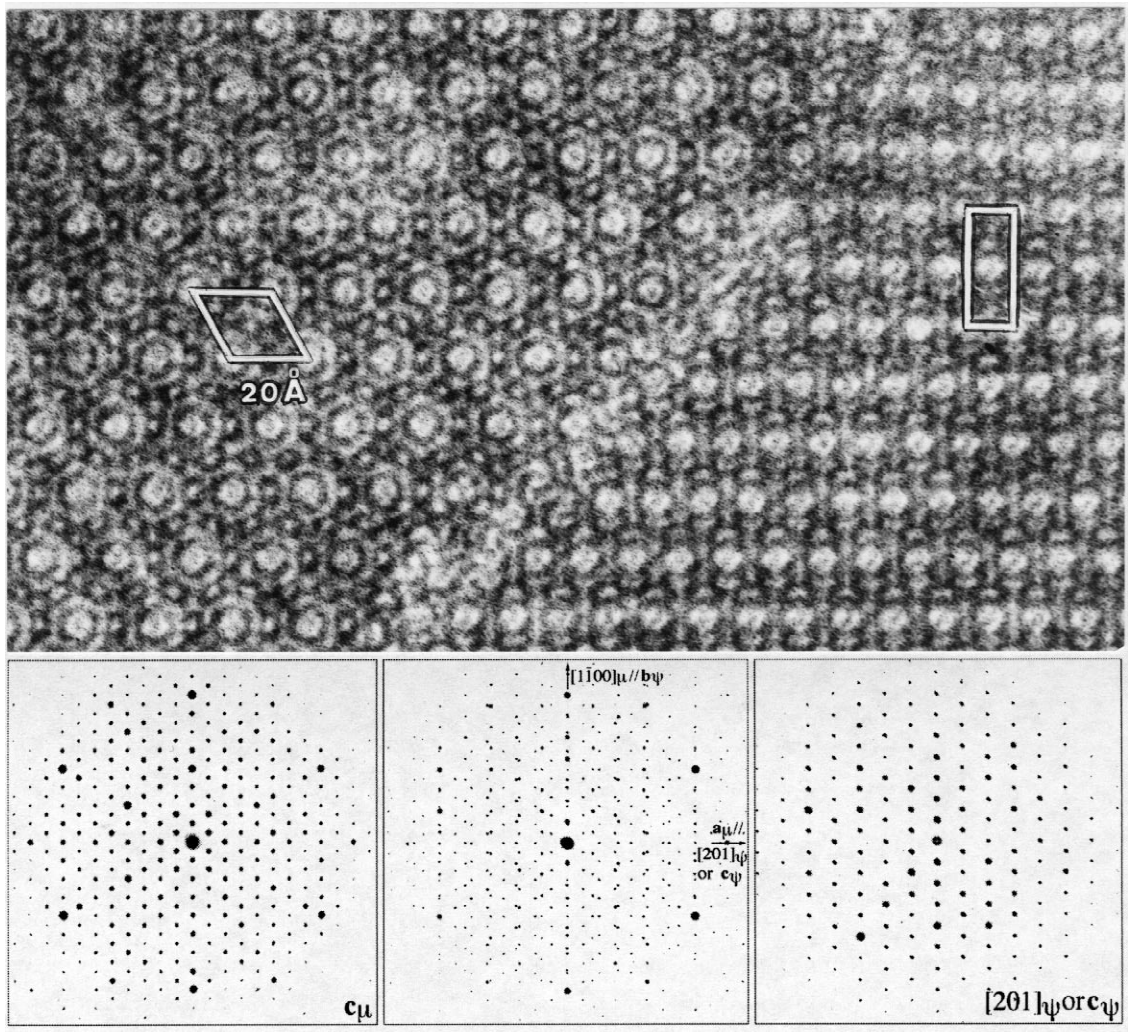

Fig. 6. μ–Ψ interface and corresponding electron diffraction patterns from which the cell parameters of the Ψ-phase were accurately determined (see Section 3.2).

4. Discussion

The close relationship observed between both the Ψ and μ phases could probably be related to a few common features between their atomic structures. Therefore, further crystallographic studies on the Ψ-phase would be interesting in order to determine whether icosahedral clusters centred on TM atoms also exist in this ternary phase structure or not (cf. Section 1).

Only intermetallic phases formed from liquid states have been reported so far. Meanwhile, in the case of the Al–Mn system, it is known that $\lambda Al_{4.5}Mn$ and $Al_{12}Mn$ phases can be obtained from solid state reactions between μAl_4Mn and Al_6Mn for $T=690°C$ and between Al_6Mn and (Al) for $T=690°C$, respectively [10–14]. Actually small proportions of λ-phase were observed in DTA Mn-rich alloy samples. For instance, a high resolution image of a λ-phase compound obtained in the $Al_{88.2}Cr_{3.8}Mn_8$ alloy is shown in Fig. 7 with the corresponding electron diffraction pattern. As we have found that the composition of this phase exhibited about the same Mn/Cr substitution ratio as the one measured for the μ-phase compound present in the same sample, it suggests that the behaviour of the Mn/Cr substitution in the λ-phase would be similar to that of the μ-phase. Such an assumption seems to be reasonable when one compares the atomic structures of both μ and λ phases whose crystallographic data have been obtained by Brink-Shoemaker et al. [22] and by Kreiner et al. [6], respectively.

According to the crystallographic data of these authors, the hexagonal cell of μAl_4Mn contains 574 atomic sites distributed on 10 and 31 Wyckoff sites for Mn and Al atoms respectively while the hexagonal cell of $\lambda Al_{4.5}Mn$ contains 586 atomic sites distributed over 15 and 51 Wyckoff sites for Mn and Al atoms respectively. There are nine of the ten Mn Wyckoff sites coordinated by icosahedra in μAl_4Mn and 14 of the 15 Mn Wyckoff sites in $\lambda Al_{4.5}Mn$. This means that within each of these

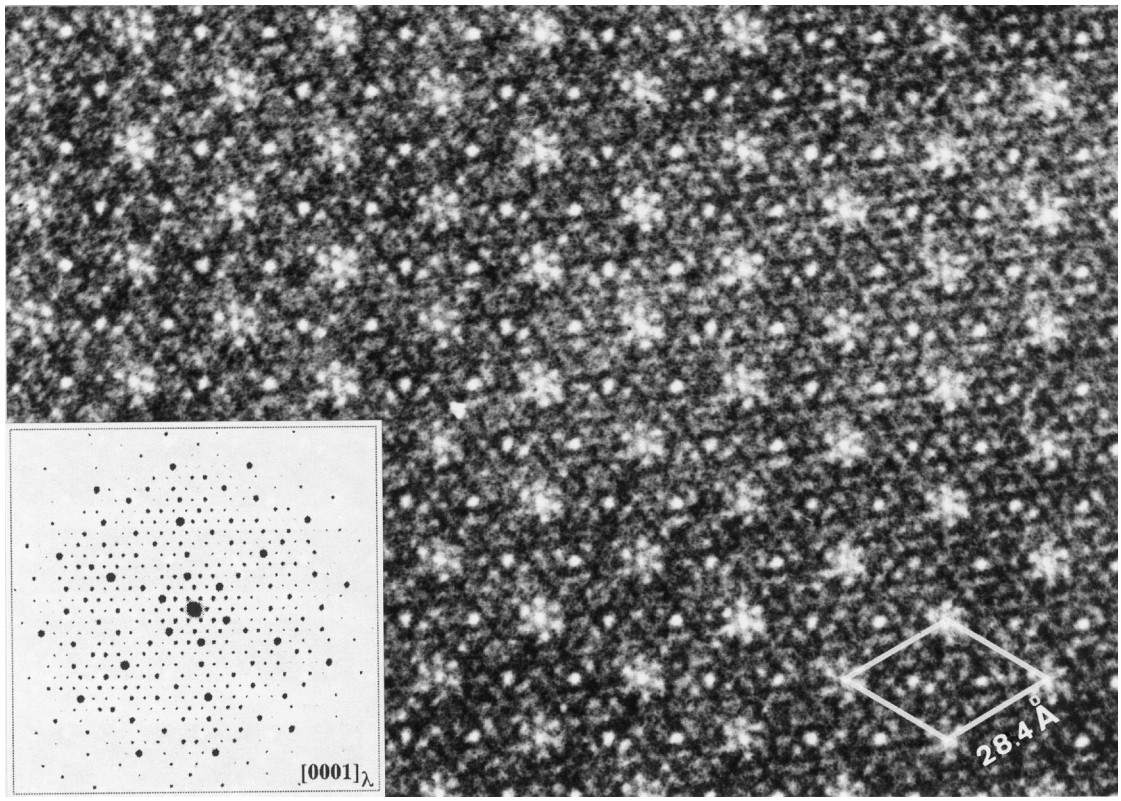

Fig. 7. High resolution image and corresponding electron diffraction pattern of [0001] zone axis of a λ-phase compound obtained in the $Al_{88.2}Cr_{3.8}Mn_8$ alloy.

structures, each Mn is surrounded by either 11Al+1Mn or 10Al+2Mn, and there is only one Mn Wyckoff site where the average coordination is of about 7Al. These last atomic sites are the Mn(1) surrounded by Al(11) with an occupancy factor of 0.424 and Al(17) with an occupancy factor of 0.672 in the report of Brink-Shoemaker et al. (1989) and the Mn(1) surrounded by Al(21), Al(22) and Al(63) with occupancy factors of 0.53, 0.4 and 0.78 respectively, in the report of Kreiner et al. [6].

Using software for drawing crystal structures, these icosahedral clusters centred on Mn atoms can be represented in order to simplify the description of these structures. Thus on account of their space groups ($P6_3/mmc$ for μ and $P6_3/m$ for λ) both these structures appear to be constituted of a stacking of icosahedral cluster layers perpendicular to the *c* axis (Fig. 8a and b). For the μ-structure, there are two flat layers centred at $z=1/4$ and $z=1/2$ (the mirror and a pseudo-mirror planes respectively) and a third corrugated layer centred at $z=3/8$. For the λ-structure, there is one flat layer centred at $z=1/4$ and a second corrugated layer is centred at $z=1/2$. The icosahedral clusters, more or less distorted with respect to the regular icosahedron, all have a twofold axis parallel to the *c* axis in the flat layers $z_\mu=1/4$, $z_\mu=1/2$, $z_\lambda=1/4$ and a threefold axis parallel to the *c* axis in the intermediate corrugated layer $z_\mu=3/8$ and $z_\lambda=1/2$. Each icosahedron is linked with first neighbours either by vertices, edges, triangular faces or through an overlap along a five-fold axis such that the Mn atom in the centre of an icosahedron stands as a vertex for a neighbouring icosahedron and vice versa. In that case, the Mn atoms represented as large white disks at the vertices of icosahedral clusters in each layer also correspond to cluster centres of the adjacent layers.

It can be pointed out in Fig. 8 that both the Mn(1) sites related to each structure have exactly the same local environment extending on a radius of about 16 Å within the layer of icosahedra at $z_\mu=1/4$ and $z_\lambda=1/4$ but also, on account of the different space groups, on a radius equal to about 6.2 Å ($=c_\mu/4=c_\lambda/2$) along the *c* axes. In other words, both these structures are related to the same arrangement of icosahedral clusters around their Mn(1) sites. Therefore, it would not be so surprising that a Mn/Cr substitution in the λ-structure could be isomorphic like in the μ-structure.

5. Concluding remarks

The occurrence of a liquid–$\mu Al_4Mn_xCr_{1-x}$ phase equilibrium for $0\leq x\leq 1$ in the Al–Cr–Mn system and with the property that the nature of the Mn/Cr substitution is isomorphic in the μ-phase can be considered as ideal for further studies on the local order of liquid alloys in

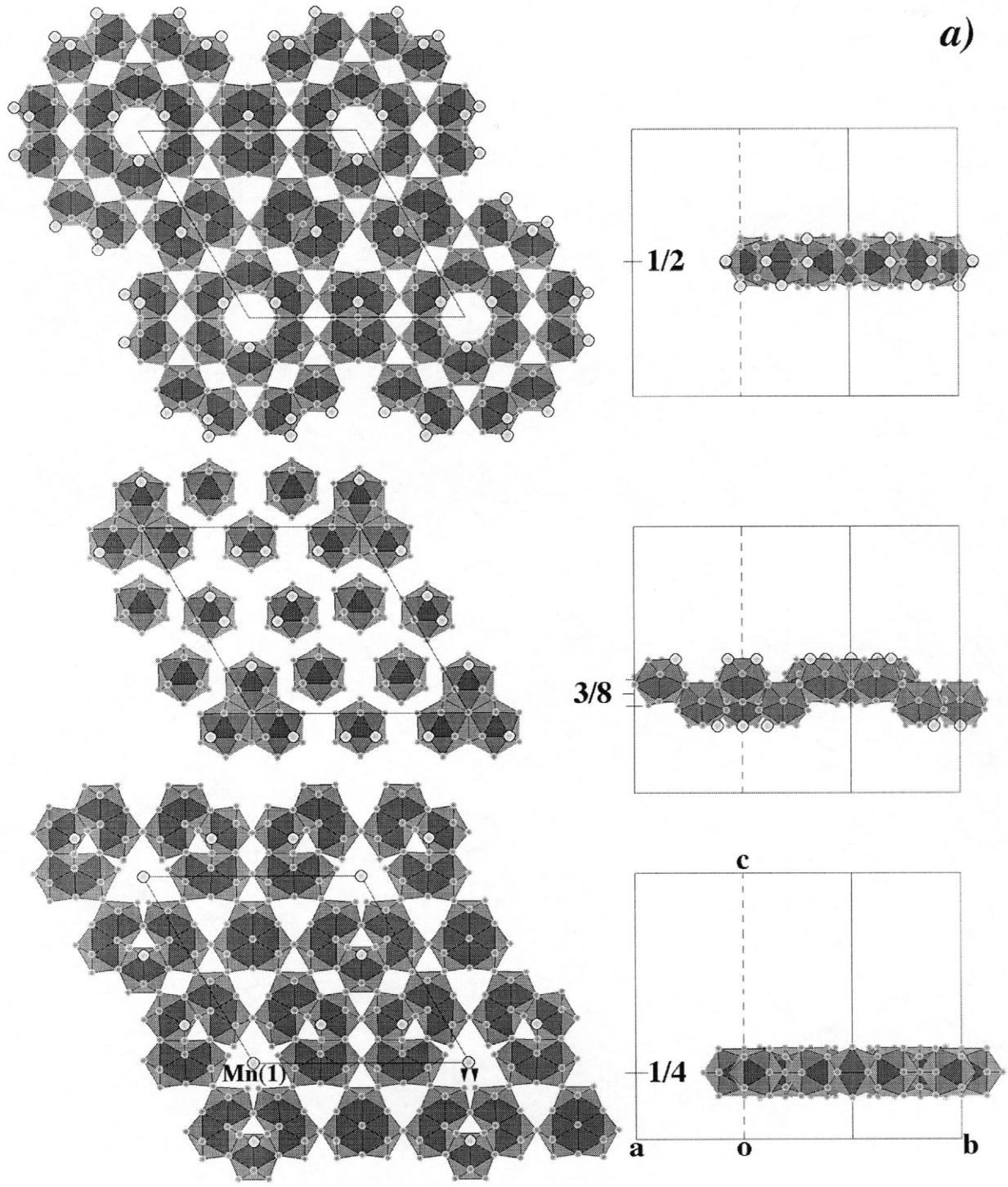

Fig. 8. Comparison of the μ (a) and λ (b) phase structures from an interpretation in terms of icosahedral clusters centred on the Mn transition metal (and according to the crystallographic data of Brink-Shoemaker et al. [21] for the μ phase and of Kreiner et al. [6], for λ phase). Al and Mn atoms at the vertices of icosahedral clusters are represented as small and large balls respectively (see Section 4). The icosahedral clusters are more or less deformed with respect to the regular icosahedron and exhibit a pseudo two-fold axis parallel to the *c* axes in the flat layers at $z_{\mu}=1/4$, $z_{\mu}=1/2$, $z_{\lambda}=1/4$ where they are either linked by vertices, triangular faces or overlap with neighbouring clusters along a pseudo five-fold axis. Al sites pointed out by arrows are too close to be simultaneously occupied. Only one Mn site in each structure (noted Mn(1)) has a coordination shell of about 7 Al instead of 12 atoms. The Mn atoms represented as large balls correspond to cluster centres situated in the adjacent layers. In the corrugated layers $z_{\mu}=3/8$ and $z_{\lambda}=1/2$, the clusters exhibit the same orientation with a three-fold axis parallel to the ***c*** axes. Some clusters are linked by edges.

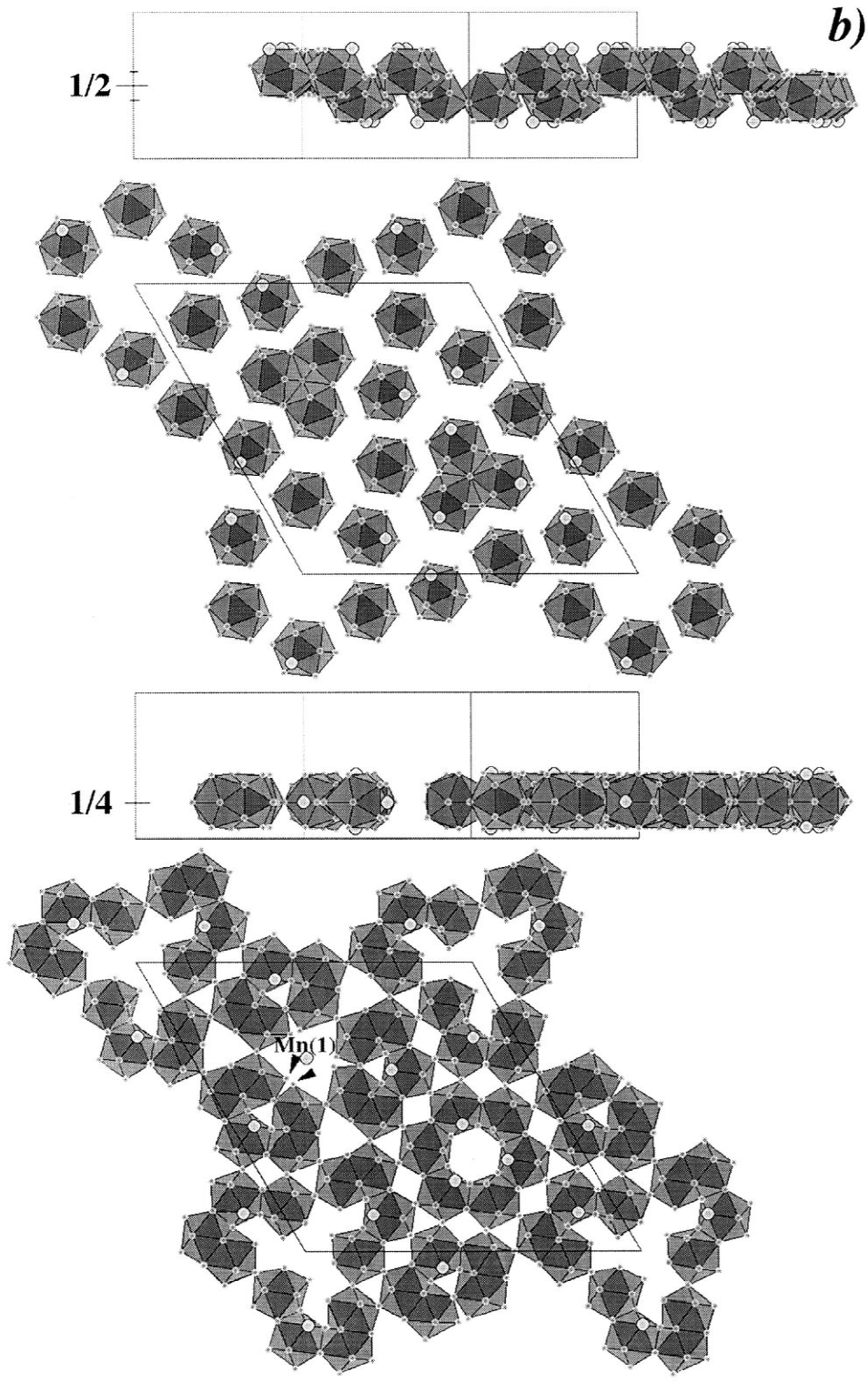

Fig. 8. (*continued*)

equilibrium with the $\mu Al_4Mn_xCr_{1-x}$ phase. In fact, these results constitute convincing arguments for inferring that an isomorphic substitution also occurs in these liquids. A local icosahedral order might be expected in these liquids because the μ-phase structure exhibits such a type of local order.

Finally, note that the Al–Mn–Cr system could also be very promising for fundamental research works on various

physical properties. For instance, as shown in a previous study [26] a localized magnetic behaviour of the μ-phase has been attributed to the presence of the TM site which does not have a local icosahedral environment (i.e. the Mn(1) site shown in Fig. 8a). The fact that the λ-structure exhibits the same site offers an opportunity for experimenting a comparison of their magnetic behaviour as magnetic properties also depend on medium and long distance correlation effects between magnetic atoms.

References

[1] S. Samson, in: A. Rich, N. Davidson (Eds.), Structural Chemistry and Molecular Biology, Freeman, San Franscisco, 1968, pp. 687–717.
[2] S. Samson, Materials Science Forum, vol. 22–24 (1987) 67–82.
[3] D.P. Shoemaker, C. Brink-Shoemaker, in: M.V. Jaric (Ed.), Aperiodic Crystals, Academic Press, Boston, 1988, ch. 1.
[4] D.P. Shoemaker, C. Brink-Shoemaker, Materials Science Forum, vol. 22–24 (1987) 83–102.
[5] D. Shechtman, I. Blech, D. Gratias, J.W. Cahn, Phys. Rev. Lett. 53 (1984) 1951.
[6] G. Kreiner, H.F. Franzen, J. Alloys Compounds 261 (1997) 83.
[7] X.Z. Li, K. Hiraga, A. Yamamoto, Phil. Mag. B 76 (1997) 657.
[8] H.X. Sui, X.Z. Liao, K.H. Kuo, X. Zou, S. Hovmöller, Acta Cryst. B 53 (1997) 587.
[9] X.G. Gong, V. Kumar, Phys. Rev. B50 (1994) 17701.
[10] F. Hippert, M. Audier, H. Klein, R. Bellissent, D. Boursier, Phys. Rev. Lett. 76 (1996) 54.
[11] A.M. Bratkovsky, A.V. Smirnov, D. Nguyen Manh, A. Pasturel, Phys. Rev. B 52 (1995) 3056.
[12] G. Trambly de Laissardière, D. Mayou, D. Nguyen Manh, Europhys. Lett. 21 (1993) 25.
[13] G. Trambly de Laissardière, D. Mayou, Magnetic Properties of Quasicrystals and Approximants, Summer School Quasikristalle, Chemnitz, 1–12 Sept. 1997 (in press).
[14] G. Trambly de Laissardière, D. Mayou, Phys. Rev. Lett. (submitted).
[15] M. Maret, P. Chieux, J.M. Dubois, A. Pasturel, J. Phys.: Condens. Matter 3 (1991) 2801.
[16] M. Maret, F. Lançon, L. Billard, Physica B 180–181 (1992) 854.
[17] M. Maret, J.M. Dubois, P. Chieux, J. Non-cryst. Solids 156–158 (1993) 918.
[18] A.J. McAlister, J.L. Murray, Bull. Alloy Phase Diagrams 8 (1987) 438.
[19] M. Harmelin, S. Maamar, S.G. Fries, H.L. Lukas, Z. Metallkd. 85 (1994) 813.
[20] J.L. Murray, in: T.B. Massalski (Ed.), Binary Alloy Phase Diagrams, ASM International, Metals Park, OH, 2nd ed., 1990, pp. 138–140.
[21] M. Audier, M. Durand-Charre, E. Laclau, H. Klein, J. Alloys Compounds 220 (1995) 225.
[22] C. Brink-Shoemaker, D.A. Keszler, D.P. Shoemaker, Acta Cryst. B45 (1989) 13.
[23] L. Bendersky, J. Microscopy 146 (1987) 303.
[24] L. Bendersky, R.S. Roth, J.T. Ramon, D. Shechtman, Metall. Trans. A22 (1991) 5.
[25] K.Y. Wen, Y.L. Chen, K.H. Kuo, Metall. Trans. A 23 (1992) 2437.
[26] T. Schenk, H. Klein, M. Audier, V. Simonet, F. Hippert, J. Rodriguez-Carvajal, R. Bellissent, Phil. Mag. Lett. 76 (1997) 189.
[27] J.L. Pouchou, F. Pichoir, Microbeam Anal. (1990) 120.
[28] J. Adam, Acta Cryst. 7 (1954) 813.
[29] A.D. Nicol, Acta Cryst. 6 (1953) 285.
[30] X.Z. Li, K.H. Kuo, Phil. Mag. B. 65 (1992) 525.
[31] M.A. Taylor, Acta Cryst. 12 (1953) 393.
[32] K. Hiraga, M. Kancko, Y. Matsuo, S. Hashimoto, Phil. Mag. B 67 (1993) 193.
[33] A. Kontio, E.D. Stevens, P. Coppens, R.D. Brown, A.E. Dwight, J.M. Williams, Acta Cryst. B 34 (1980) 435.
[34] J. Cooper, Acta Cryst. 13 (1960) 257.
[35] M. Ellner, J. Braun, B. Predel, Z. Metallkd. 80 (1989) 374.
[36] J. Rodriguez-Carvajal, FULLPROF program (Version 3.1c Jan 96-LLB-JRC).
[37] H.M. Rietveld, Acta Cryst. 22 (1967) 151.
[38] H.M. Rietveld, J. Applied Cryst. 2 (1969) 65.